

ARTICLE

Fitting individual-based models of spatial population dynamics to long-term monitoring data

Anne-Kathleen Malchow¹  | Guillermo Fandos^{1,2}  | Urs G. Kormann³  |
Martin U. Gruebler³  | Marc Kéry³  | Florian Hartig⁴  | Damaris Zurell¹ 

¹Institute for Biochemistry and Biology,
University of Potsdam, Potsdam,
Germany

²Department of Biodiversity, Ecology and
Evolution, Complutense University of
Madrid, Madrid, Spain

³Swiss Ornithological Institute, Sempach,
Switzerland

⁴Theoretical Ecology, Faculty of Biology
and Pre-Clinical Medicine, University of
Regensburg, Regensburg, Germany

Correspondence

Anne-Kathleen Malchow

Email: eco@anne-kathleen.malchow.nz

Funding information

Deutsche Forschungsgemeinschaft,
Grant/Award Number: ZU 361/1-1

Handling Editor: Colin J. Torney

Abstract

Generating spatial predictions of species distribution is a central task for research and policy. Currently, correlative species distribution models (cSDMs) are among the most widely used tools for this purpose. However, a fundamental assumption of cSDMs, that species distributions are in equilibrium with their environment, is rarely fulfilled in real data and limits the applicability of cSDMs for dynamic projections. Process-based, dynamic SDMs (dSDMs) promise to overcome these limitations as they explicitly represent transient dynamics and enhance spatiotemporal transferability. Software tools for implementing dSDMs are becoming increasingly available, but their parameter estimation can be complex. Here, we test the feasibility of calibrating and validating a dSDM using long-term monitoring data of Swiss red kites (*Milvus milvus*). This population has shown strong increases in abundance and a progressive range expansion over the last decades, indicating a nonequilibrium situation. We construct an individual-based model using the RangeShiftR modeling platform and use Bayesian inference for model calibration. This allows the integration of heterogeneous data sources, such as parameter estimates from published literature and observational data from monitoring schemes, with a coherent assessment of parameter uncertainty. Our monitoring data encompass counts of breeding pairs at 267 sites across Switzerland over 22 years. We validate our model using a spatial-block cross-validation scheme and assess predictive performance with a rank-correlation coefficient. Our model showed very good predictive accuracy of spatial projections and represented well the observed population dynamics over the last two decades. Results suggest that reproductive success was a key factor driving the observed range expansion. According to our model, the Swiss red kite population fills large parts of its current range but has potential for further increases in density. We demonstrate the practicality of data integration and validation for dSDMs using RangeShiftR. This approach can improve predictive performance compared to cSDMs. The workflow presented here can be adopted for any

This is an open access article under the terms of the [Creative Commons Attribution](https://creativecommons.org/licenses/by/4.0/) License, which permits use, distribution and reproduction in any medium, provided the original work is properly cited.

© 2024 The Authors. *Ecological Applications* published by Wiley Periodicals LLC on behalf of The Ecological Society of America.

population for which some prior knowledge on demographic and dispersal parameters as well as spatiotemporal observations of abundance or presence/absence are available. The fitted model provides improved quantitative insights into the ecology of a species, which can greatly aid conservation and management efforts.

KEYWORDS

Bayesian inference, cross-validation, dispersal, inverse calibration, process-based model, range dynamics, spatially explicit, species distribution model (SDM)

INTRODUCTION

In response to multiple anthropogenic pressures and environmental shifts, the abundance and distribution of many species are changing (Díaz et al., 2019; Newbold et al., 2015; Selwood et al., 2015). Decreasing populations may be stabilized or even recover by effective conservation measures (Bolam et al., 2021; Duarte et al., 2020; Hoffmann et al., 2010). But expanding populations can also be the focus of conservation interest, for example when exploring scenarios of future threats or evaluating the invasive potential of a species (Thompson et al., 2021). The basis for efficient conservation planning thus lies in reliable knowledge about the spatiotemporal patterns of abundance and the expected effects of conservation measures (Guisan et al., 2013; Zurell et al., 2022).

Various approaches have been developed for spatially explicit population modeling, ranging from purely correlative to detailed mechanistic species distribution models (SDMs; Dormann et al., 2012; Guisan et al., 2013). Currently, most spatial model assessments for conservation planning are based on projections of correlative SDMs (cSDMs) (Franklin, 2013; Zurell et al., 2022), which statistically relate species occurrences to environmental predictors (Elith & Leathwick, 2009). This class of models can achieve high flexibility and may be readily fitted to available occurrence data, but their geographical and temporal transferability is limited (Araújo & Peterson, 2012; Wenger & Olden, 2012). Furthermore, they only provide stationary or time-implicit projections, which rely on the assumption that the observed distribution stays in equilibrium with its environment, even if the environmental conditions change (Guisan & Thuiller, 2005). However, this assumption is commonly violated in conservation-relevant cases, such as for invasive species, in reintroduction programs, or for threatened populations affected by ongoing environmental change. This leads to inaccurate predictions because the true species distribution is actually transient and, thus, dependent on time and history (Santos et al., 2020; Semper-Pascual et al., 2021; Watts et al., 2020).

Such dynamic abundance patterns can be represented with spatially explicit process-based SDMs (hereafter called dSDMs). These models explain present species distributions and abundances as the result of interacting ecological processes, such as demography, dispersal, and evolution (Urban et al., 2016). To this end, dSDMs explicitly describe at least one of these processes to model spatiotemporal and potentially transient population dynamics. Examples include representations of local population dynamics (Barber-O'Malley et al., 2022; Keith et al., 2008) and limiting processes like dispersal (Broms et al., 2016; Hefley et al., 2017; Risk et al., 2011; Smolik et al., 2010; Wikle, 2003), physiology (Rodríguez et al., 2019), or species interactions (Pellissier et al., 2013; Schweiger et al., 2012). Further, dSDMs often include stochastic elements to account for processes not explicitly described by the model or for intrinsic variability. Thanks to the integration of ecological theory, dSDMs are expected to provide more accurate predictions under extrapolation and, thus, to be more readily transferable to nonanalog conditions than cSDMs (Gallien et al., 2010).

A challenge for working with dSDMs is their specification and validation (Schmolke et al., 2010). Fully specifying a dSDM includes two main steps, both of which require distinct types of knowledge about the population of interest (Singer et al., 2018; Figure 1). First, in the model building step, the model structure and the functional description of the relevant processes are established. Both are usually chosen based on ecological theory and expert opinion. Second, in the parameterization step, the numeric values of all model parameters, such as demographic and dispersal rates, are determined by direct or inverse (also called indirect) parameterization or a combination of both. Direct parameterization uses estimates of process parameters based on data collected in the field or from experiments. Inverse parameterization determines likely parameter values by comparing the generated model response, typically spatiotemporal abundance or occurrence, with observed field data. To make efficient use of all sources of information and combine both direct and inverse parameterization, a

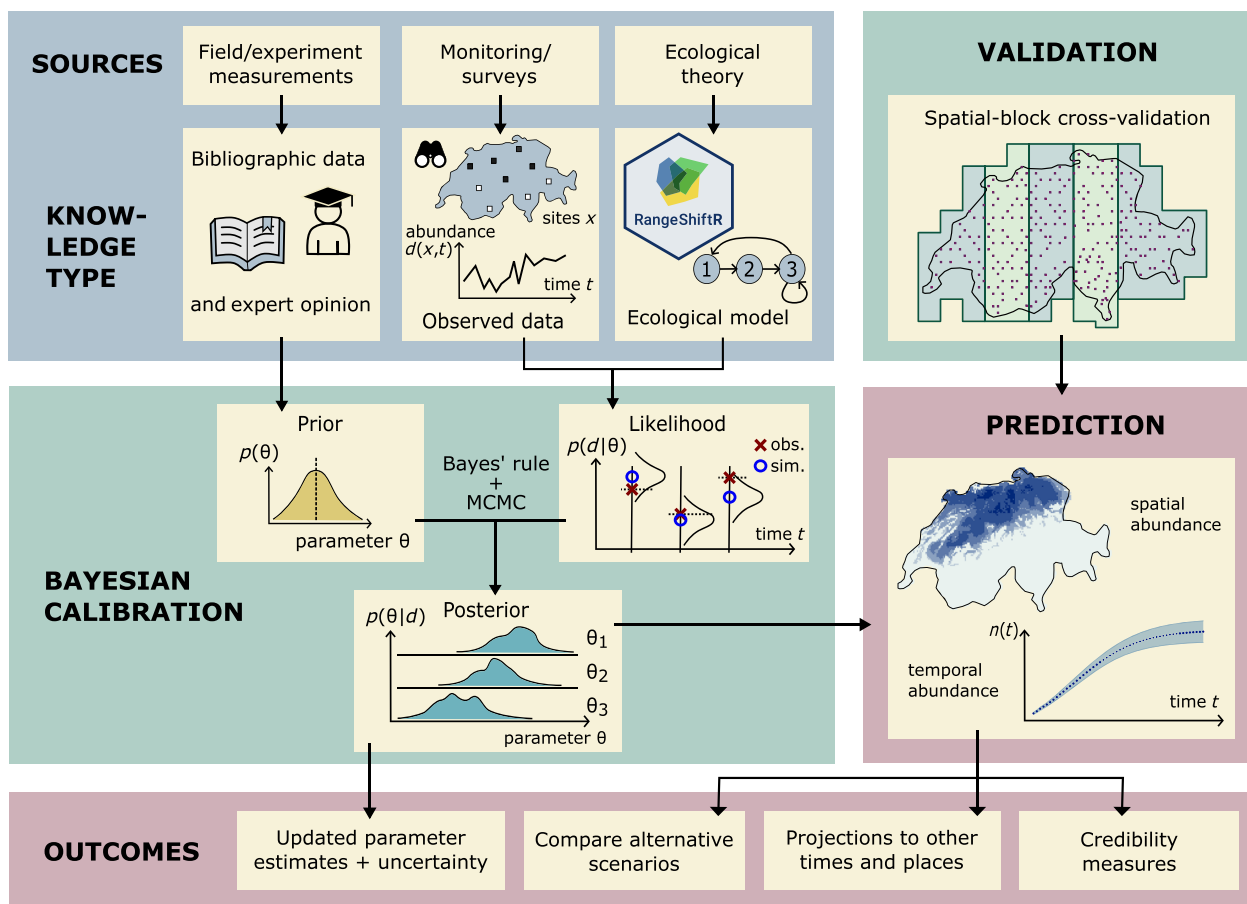


FIGURE 1 Calibration and validation workflow for process-based, dynamic distribution and population models. Different types of knowledge are needed to specify the model structure and parameterization. Their direct specification can be informed from literature data, expert opinion, and ecological theory. In a calibration, the direct knowledge on model parameters is combined with observations of the modeled response. When using Bayesian inference, this is done via the likelihood function evaluated for these data. For cross-validation, the calibration is repeated for different subsets of data using the held-out data to measure predictive performance. Multiple outcomes can be derived, both from the posterior distribution directly and from model projections. Obs., Observed; Sim., Simulated.

Bayesian calibration framework can be employed. In this, the direct parameterization and its uncertainty are expressed as prior distributions. The prior is updated via Bayes' rule using a likelihood that measures how well a given set of parameter values is able to reproduce the observed response data. This updated prior yields the posterior distribution (Hobbs & Hooten, 2015). The procedure thus identifies parameterizations that are consistent with the data and can generate new knowledge on the studied population, as prior estimates of process parameters are modified by new data and their uncertainty may be reduced. This approach further allows the consistent propagation of uncertainty from the data sources through to model projections (Hartig et al., 2012; Jaatinen et al., 2021; Marion et al., 2012). Ultimately, in the validation step, the predictive performance of the specified model is assessed. For this, the model is evaluated on a set of testing data that, ideally, is independent of the training data. One way to generate the training and testing data is

cross-validation, in which the full data set is partitioned in a prescribed way, for example, in leave-p-out or k-fold cross-validation (Arlot & Celisse, 2010). The final, validated model can be used to generate projections to other times or places and to compare the outcome of alternative management scenarios (Bleyhl et al., 2021).

Despite repeated calls for more dSDM approaches, the widespread use of dSDMs for conservation applications has been hampered by technical challenges with respect to their parameterization and validation (Briscoe et al., 2019). With the proliferation of novel methods for the various model building steps, software tools are being developed that assist their case-specific implementation. In R, these are available as packages for building different types of complex dSDMs (Fordham et al., 2021; Hagen et al., 2021; Landguth et al., 2017; Malchow et al., 2021; Moulin et al., 2021; Visintin et al., 2020), for model calibration (Csilléry et al., 2012; Hartig et al., 2019), and for cross-validation (Valavi et al., 2019). However, their

combined application in integrated modeling workflows is still challenging and rarely done.

In this study, we present a complete calibration and validation workflow for dSDMs, utilizing heterogeneous data for direct and inverse parameterization. As a case study, we modeled the Swiss population of red kite (*Milvus milvus*). This population has a highly dynamic recent history with accelerating increases over the last 50 years (Aebischer & Scherler, 2021), rendering a dynamic modeling approach adequate. We first built a dSDM with the individual-based modeling (IBM) platform RangeShiftR, which explicitly simulates the processes of population dynamics and dispersal (Malchow et al., 2021). Then, its process parameters were directly parameterized using published literature data (Appendix S1: Table S1). This direct parameterization was subsequently updated by integrating information from long-term, structured survey data with Bayesian inference using the R package BayesianTools (Hartig et al., 2019). Finally, the predictive performance of the calibrated model was evaluated by cross-validation on spatially blocked data folds (Roberts et al., 2017). To test our workflow, we investigated whether the calibration could successfully inform parameter estimates and which process parameters were most sensitive to the survey data. Comparing the prior and posterior predictive distributions under our model, we assessed whether the calibration improved model fit and reduced uncertainty. Predictive performance of the fitted model was evaluated in a spatial-block cross-validation and compared to a cSDM fitted to the same data. Lastly, the calibrated model was used to explore the potential population size and distribution of red kite in Switzerland.

Our workflow (Figure 1) is intended to guide the application of complex dSDMs to populations with nonstationary dynamics. Variable dynamics, such as substantial increases or decreases, possibly interspersed with constant phases, are needed to disentangle the dynamic processes that constitute a dSDM. This requires the availability of suitable data sources for direct and inverse parameterization. Using formal methods for calibration, validation, and uncertainty quantification, our workflow links process-based models with monitoring data to produce a sound quantitative basis for management decisions that is explicit about all uncertainties involved (Zylstra & Zipkin, 2021).

MATERIALS AND METHODS

Data

We utilized two sources of monitoring data of the red kite in Switzerland: the Swiss breeding bird atlas that

provides snapshot data from two periods (1993–1996) (Schmid et al., 1998; and 2013–2016, Knaus et al., 2018) and the Swiss common breeding bird survey (MHB, by its German initials) (Schmid et al., 2004), which provides abundance time series for every year since 1999. We used the MHB series up to the year 2019. Both schemes are based on so-called simplified territory mapping of a systematic-random sample 1-km² squares across Switzerland and record the number of observed breeding pairs (BPs) during two to three repeat surveys per breeding season along a fixed survey route of typically 4–6 km in each square (Schmid et al., 2004). The atlas survey data used here included 2318 sites, each of which was sampled in 1 year within each 5-year period, while the MHB survey included 267 sites sampled annually. Further, we used land-cover and bioclimatic data as environmental predictors. Land cover was represented with the CORINE Land Cover (Copernicus Land Monitoring Service, 2022) classification (44 classes), obtained for the years 2000, 2006, 2012, and 2018 at a spatial resolution of 100 m. Climate was represented by the 19 WorldClim bioclimatic variables. We used averaged annual values from the time period 1979–2013 with a spatial resolution of 30 arcsec (~1 km) obtained from CHELSA Bioclim version 1.2 (Karger et al., 2017; Karger, 2018). An overview of all data sources and their use in the modeling process is given in Appendix S1: Tables S1–S3.

Modeling

Our dSDM comprised two components, which are detailed in the following section: (1) a static habitat model that describes the habitat suitability in each year over the study region and (2) a mechanistic IBM (Railsback & Grimm, 2019) that describes the population and range dynamics. IBMs use a bottom-up approach in which key processes are formulated at the individual level and are scaled up to the population level by numerical simulation (DeAngelis & Mooij, 2005). All analyses were conducted using the statistical programming language R (R Core Team, 2020) and several R packages (see below).

Habitat suitability of Swiss landscape

Habitat suitability was derived from a cSDM based on presence–absence data from the second atlas (2013–2016) data set. Because the red kite has been expanding its range in Switzerland during the past 50 years, these most recent data best reflect the underlying habitat requirements. For the cSDM, we assumed that most suitable

habitats were already occupied, even though they might not have reached their potential capacities yet. The red kite is a generalist and opportunistic raptor that breeds in a wide range of climates and habitats. Its typical nesting habitat consists of forest patches with suitable roosting sites and adjacent open areas like grassland or agricultural fields that provide prey, which mostly consists of small mammals. Food sources like open waste dumps and carrion are readily exploited where present. To represent the availability of resources relevant for the occurrence of red kites, we used the CORINE 2012 land cover data (Copernicus Land Monitoring Service, 2022) and aggregated its 44 classes to seven land cover types (Appendix S1: Table S2). To represent climatic influences, all 19 Bioclim variables were included (Appendix S1: Table S3). Since the red kite requires different habitats for nesting and foraging, it is a mobile species and occupies breeding home range sizes of about 4–5 km² for males (Baucks, 2018; Nachtigall, 2008). To allow the cSDM to consider the diversity of habitat types, we used a grid cell size of 4 km². Since the IBM was based on the same grid, this also constitutes a trade-off between the abilities to resolve both the effects of density dependence on the one hand and dispersal displacements on the other. The high-resolution land cover data were aggregated to the target resolution of 2 km by calculating the proportional land cover in each cell. The bioclimatic data were coarsened to the 2-km resolution by bilinear interpolation between the grid cells.

To fit the cSDM habitat model, we first selected predictors from all land-cover and bioclimatic variables based on their univariate importance (assessed by the AIC of linear models with second-order polynomials) under the constraint that pairwise Spearman correlations must not exceed 0.7 (Dormann et al., 2013). The variables selected are labeled with an asterisk in Appendix S1: Tables S2 and S3. We then created an ensemble cSDM by taking the mean occurrence probability predicted by four different algorithms: binomial linear model with second-order polynomials and stepwise variable selection; binomial additive model with splines; random forest; and boosted regression trees. The predicted probabilities are subsequently interpreted as a habitat suitability index (HSI). The ensemble cSDM was then projected to Switzerland and a 12-km buffer around its border in the years 2000, 2006, 2012, and 2018, with varying land-cover data and constant bioclimatic variables. Climate was kept constant because it was considered only a minor driver of change in resource availability over the study period. The buffer was applied to reduce potential boundary effects in the IBM simulations. It was large enough to capture most dispersal events in the Swiss population. For all other years in the period of 1999–2019, the HSI values were linearly interpolated. To

distinguish between habitat and nonhabitat cells, we derived a banalization threshold ($\widehat{\text{HSI}} = 0.51$) as the value yielding equal sensitivity and specificity ($\approx 90\%$) and considered all cells with lower HSI values nonhabitat.

IBM

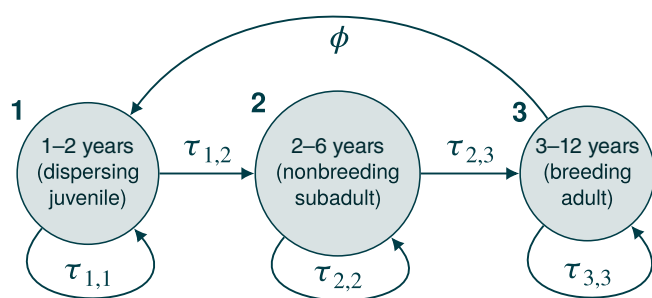
We used the R package RangeShiftR (Malchow et al., 2021), which is an interface to the individual-based modeling platform RangeShifter 2.0 (Bocedi et al., 2021), to construct a dSDM based on the gridded habitat suitability maps described above. Next, we describe the main steps of the direct parameterization and refer to the full Overview, Design concepts, Details (ODD) protocol (Grimm et al., 2020) in Appendix S2 for all details. RangeShiftR explicitly simulates demography and dispersal in discrete unit-time steps, which here comprise 1 year. During each year, the processes “reproduction,” “juvenile dispersal,” “survival,” “development,” and “aging” are evaluated in this order for all individuals. The prior distributions on the respective process parameters (Table 1) were informed by literature data (Appendix S1: Table S1) and expert knowledge. They were then updated with information contained in the survey data via Bayesian inference as described in the section Bayesian calibration.

Our model is female-based, since females primarily determine the population dynamics in red kites. Their development is described in three stages (Figure 2), with classifications and age ranges adopted from Sergio et al. (2021) and Newton et al. (1989): Dispersing juveniles are 1 or 2 years old, subadults establish a territory within their second to sixth year, and breeding adults are aged between 3 and 12 years. A senescent stage was not included in the model because it does not contribute to the overall fecundity, and nonbreeding adults are not monitored in the survey. These age limits are not strict, as the stage transitions are modeled probabilistically (Figure 2). The transition probabilities $\tau_{m,n}$ are expressed as survival probabilities of stage s , $\sigma_s = \tau_{s,s} + \tau_{s,s+1}$, and the development probabilities $\gamma_s = \tau_{s,s+1} \sigma_s^{-1}$. Both can independently vary between zero and one. The development probabilities are assumed to be $\gamma_1 = 0.80 \pm 0.10$ for Stage 1 and $\gamma_2 = 0.55 \pm 0.10$ for Stage 2, to approximately yield the described age classes (Appendix S1: Figure S1). The survival probabilities σ are taken from Katzenberger et al. (2019) for all three stages: $\sigma_1 = 0.42 \pm 0.08$ and $\sigma_2 = 0.68 \pm 0.09$ and $\sigma_3 = 0.80 \pm 0.05$, which is also in accordance with Schaub (2012) and Newton et al. (1989).

Fecundity ϕ was assumed to be density-dependent and was modeled as exponentially decaying with

TABLE 1 Process parameters of IBM included in Bayesian calibration and parameters of their truncated normal prior distributions.

Parameter name	Lower bound	Mean	SD	Upper bound
Density dependence, b^{-1}	0.001	0.006	0.0025	0.020
Fecundity, ϕ_0	0.5	1.66	0.51	5.0
Survival probability, σ_1	0.01	0.42	0.08	0.99
Survival probability, σ_2	0.01	0.68	0.09	0.99
Survival probability, σ_3	0.01	0.80	0.05	0.99
Development probability, γ_1	0.01	0.80	0.10	0.99
Development probability, γ_2	0.01	0.55	0.10	0.99
Emigration probability, e_1	0.01	0.80	0.10	0.99
Settlement inflection point, β_s	-15.0	4.0	4.0	15.0
Dispersion parameter, ν	1.0	50.0	250.0	500.0

**FIGURE 2** Life-cycle graph of population model for red kite with three developmental stages. The probability that an individual in stage s will stay in its stage over one time step (1 year) is denoted by $\tau_{s,s}$, and the probability that it will move to the next stage is denoted by $\tau_{s,s+1}$. Only Stage 3 produces offspring, with a fecundity of ϕ .

population density. Each cell i is characterized by a local strength of demographic density dependence b_i , which is obtained as the global strength b divided by the cell habitat suitability HSI_i , $b_i = b HSI_i^{-1}$, given in units of cell area ($a_c = 4 \text{ km}^2$). Fecundity follows the relation $\phi_i(n_i) = \phi_0 e^{-b_i n_i}$, where n_i denotes the density of adults in Stages 2 and 3 in cell i (i.e., juveniles do not contribute to this density dependence). The base value ϕ_0 is the required process parameter and denotes the theoretical fecundity at zero population density. Nägeli et al. (2021) report a realized fecundity of 1.77 ± 0.70 , which agrees with Schaub (2012) and Nachtigall (2008). We assumed that this value was reached at a density of 25 BPs per 100 km^2 (i.e., 1 BP per cell) and halved it for our female-only model: $\phi_1 = \phi(n = 1/a_c) = 0.88 \pm 0.35$. We can then get ϕ_0 from $\phi_0(b) = \phi_1 e^{b/HSI}$, with b as a calibration parameter that controls the strength of density-dependence in fecundity. The HSI over all habitat cells had a mean and SD of $80\% \pm 12\%$, and we assumed that the lower and higher fecundities were attained in the

lower- and higher-quality habitats. This was given with a range of $b = (0.50 \pm 0.15)a_c$ (Appendix S1: Figure S2), yielding $\phi_0 = 1.65 \pm 0.51$.

Dispersal is explicitly modeled in three stages: emigration, transfer, and settlement (Travis et al., 2012). Red kites are strongly philopatric (Newton et al., 1989), so that emigration was modeled as occurring in the first developmental stage, that is, dispersing juvenile, only. The emigration probability was assumed constant at $e_1 = 0.64 \pm 0.10$, meaning that an expected proportion of 87% of juveniles have dispersed within their first 2 years. This value best matched observations in which 42% of females of a cohort have emigrated after Year 1 and 45% after Year 2 (author's own unpublished data), suggesting a larger proportion of emigrants among 2-year-old juveniles than among 1-year-old juveniles. The transfer phase described the movement of a dispersing individual through the landscape. It was modeled as a strongly correlated random walk in a random direction with a step length equal to the cell size. After each step, the option to end the movement and settle in a cell for future breeding site was evaluated. Settlement was only possible in habitat cells, and its probability was density-dependent with a sigmoid relationship (Appendix S1: Figure S3). Its inflection point β_s was a calibrated parameter and was estimated as $\hat{\beta}_s = \beta_s/b = (4 \pm 4)a_c^{-1}$. The maximum settlement probability and the slope parameter were fixed at $\alpha_s = -1$ and $s_0 = 0.75$, respectively, in order to reduce flexibility. At these values, the choice of just β_s makes it possible to tune the density-dependent settlement across a wide range of reasonable relationships (Appendix S1: Figure S3). The maximum number of steps in the random walk was set to 10. Therefore, depending on the availability of sparsely populated habitat, individuals exhibit dispersal distances between 2 and a maximum of 20 km, which is consistent with observations (authors' own unpublished data; Nachtigall, 2008; Newton et al., 1989).

Longer-range dispersal events are also frequently observed, but they were excluded from the model due to the small study region and the mountainous terrain. Immigration or emigration of individuals across the system boundaries was not considered.

The initial conditions of each simulation were stochastic. The number of adult individuals in each cell was drawn from a Poisson distribution whose mean values were predicted from a generalized linear model. This model of the initial red kite distribution was an autoregressive distribution model (Dormann et al., 2007) of the earlier atlas data (1993–1996) with the spatially interpolated values of atlas counts as its sole predictor (Appendix S1: Figure S4). The number of juveniles and subadults was subsequently estimated from the demographic rates under the assumption of a stable stage distribution.

Bayesian calibration

We used Bayesian inference to evaluate the joint posterior distribution of nine model parameters θ based on their prior distributions $p(\theta)$ and the likelihood $l(\theta)$ (Figure 1). The priors express the a priori information that we assumed about likely parameter values as summarized in Table 1. The likelihood function $l(\theta)$ measures the fit of a model M , parameterized with θ , to the monitoring data. The estimated model parameters are as follows: strength of density dependence $1/b$; six demographic probabilities for survival of all stages (σ_1 , σ_2 , σ_3), juvenile and subadult development (γ_1 , γ_2), and base adult fecundity (ϕ_0); and two dispersal parameters to control emigration (e_1) and settlement probabilities (β_s). Additionally, we calibrated a dispersion parameter ν , which is introduced in what follows.

As priors $p(\theta)$ we chose truncated normal distributions for all parameters. Their means and SDs were informed from the literature and expert opinion, and they were bounded to their respective valid parameter ranges (Table 1). As calibration data, we used observed abundances from the MHB survey, D_{MHB} . Based on these data, we defined a likelihood $l(\theta) = p(D_{\text{MHB}} | \theta, M)$ as follows: For a given parameter vector θ , the RangeShiftR simulation model (M) was run and the output abundance data were aggregated and averaged over 20 replicate runs of the model. The result D_{sim} was compared with the MHB counts under the assumption of a negative-binomial (NB) error distribution, so that for an observation at site i and time t , $l_{i,t}(\theta) = \text{Pr}_{\text{NB}}(D_{\text{MHB},i,t} | \mu = D_{\text{sim},i,t}, \nu)$. The parameter ν describes the error overdispersion and was also estimated

from the data. It arises in an alternative formulation of the NB probability mass function Pr_{NB} formulated in terms of its mean μ and dispersion ν , instead of the more common success probability $r = \nu\mu + \nu$ and the target number of successes $n = \nu$. Therefore, its variance is given by $\sigma^2 = \mu + \mu^2\nu$. It approaches μ from above when $\nu \rightarrow \infty$, as the NB converges to the Poisson distribution. The amount of overdispersion can thus be tuned by the value of ν , rendering Pr_{NB} an appropriate error description for potentially overdispersed count data.

Due to the stochasticity inherent in our simulation model, the likelihood values calculated from repeat simulations were still stochastic to some extent. They thus represent an estimator of the exact likelihood. Conceptually, this is not a problem for our Markov chain Monte Carlo approach (MCMC, details below), since the pseudo-marginal theorem guarantees that the MCMC sample still converges to the exact posterior distribution (Andrieu & Roberts, 2009). In practice, however, large variances in the likelihood estimator can increase the time required for MCMC convergence dramatically when the sampler gets stuck at occasional high values. To reduce the variance in the likelihood estimates, we aggregated the abundance data within spatiotemporal blocks of 14×14 grid cells in space and 3 years in time (Appendix S1: Figures S5 and S6). These aggregation factors were chosen with the target of reaching a variance below 10 on the logarithmic scale in repeated likelihood evaluations for a given θ (Appendix S1: Figure S7). The aggregation resulted in 57 spatial and five temporal blocks, within which the observed and simulated red kite densities were compared. Under the usual independence assumption, the total likelihood was then expressed as the product over all such blocks: $l(\theta) = \prod_{i=1}^{57} \prod_{t=1}^5 l_{i,t}(\theta)$.

To validate the calibration setup and assess the sensitivity of the likelihood $l(\theta)$ to changes in the model parameters θ , we performed a local sensitivity analysis (Appendix S1: Figure S7). For this, a test data set D_{SA} was simulated from the model with all parameters at their mean prior values. Then one parameter at a time was varied within the boundaries of its prior distribution while keeping all other parameters at their mean and estimating the likelihood with respect to D_{SA} . Further, we performed a global sensitivity analysis with Morris' elementary effects screening method (Morris, 1991).

To estimate the joint posterior distribution based on the defined $p(\theta)$ and $l(\theta)$, we used a MCMC sampling scheme (Luengo et al., 2020). Therein, the posterior density $p(\theta | D_{\text{MHB}}, M)$ of a series of given parameter sets θ was evaluated according to Bayes' rule. The utilized MCMC algorithm was a variant of the adaptive Metropolis sampler, namely, the differential evolution sampler

with snooker update (DEzs, ter Braak & Vrugt, 2008), as implemented in the BayesianTools R package (Hartig et al., 2019). Every calibration run included three independent DEzs-MCMC instances with a length of 2×10^5 iterations, of which the first 5×10^4 were discarded as burn-in. Each DEzs, in turn, consisted of three interdependent internal chains, so that each calibration comprised a total of nine chains. The chains were checked for convergence using trace plots, trace rank plots (Vehtari et al., 2021), and the multivariate potential scale reduction factor (PSRF; Gelman and Rubin (1992)). A chain was considered approximately converged if its multivariate PSRF value dropped below 1.10 and the trace and trace rank plots showed well-mixed chains.

To assess the information gained in the calibration, the sampled posterior distributions were contrasted with the prior distribution. To this end, the parameter estimates were compared with respect to the medians and quantiles of their respective marginal distributions. To evaluate whether and by how much the uncertainty was reduced, we assessed and compared the distribution breadth by calculating the width of the highest-posterior-density intervals (HPDIs).

Cross-validation and prediction

We employed a spatial-block cross-validation scheme to evaluate the model fit without duplicate use of data for both model calibration and validation (Roberts et al., 2017). To this end, the data were split into five spatially contiguous folds (Figure 1 and Appendix S1: Figure S5). For each fold, the respective subset of MHB data were held out and the model was fit to the remainder of the data. To ensure that the folds covered largely identical spaces of environmental conditions, we chose longitudinally structured folds that included a similar altitudinal profile. For model validation, the respective calibration results for each fold were used. For final model projections, in turn, a separate calibration on the full data set was used.

Posterior model predictions were generated by taking a sample of 1000 draws from the joint posterior, running the dSDM with each drawn parameter vector, and calculating the mean, median, and 95% credibility interval of the simulated abundances. Prior predictions were obtained in the same way but using draws from the prior distribution. Both prior and posterior predictions were run for the time covered by the MHB data and additional 30 years forward with constant habitat suitabilities, that is, no changes in land cover or climate were considered. This projection provides an estimate of the potential current population size

and distribution, without making a prediction as to future conditions.

To assess the model's predictive performance, we calculated, using the function "rcorr.cens" from the Hmisc R package, Harrell's *c*-index (Newson, 2006), a rank correlation index that generalizes the area under the receiver-operating-characteristic curve (AUC) index to nonbinary response variables. It quantifies the probability that for a given pair of data points the ranking of predictions will match the ranking of observations. This measure was used in Briscoe et al. (2021) as a form of temporal AUC to assess the fit to temporal trends. We used it here as an index that was applicable to abundance projections and could be interpreted like the AUC for occurrence projections.

RESULTS

Sensitivity analysis

Based on the local and global sensitivity analyses (Appendix S1: Figures S7 and S8), we found that the likelihood estimates responded most strongly to variations in the strength of density dependence $1/b$, the adult base fecundity ϕ_0 , and the three survival probabilities σ_1 , σ_2 , and σ_3 . Therefore, we expected that these parameters would calibrate best under our setup, while the development probabilities γ_1 , γ_2 and the emigration probability e_1 would be only weakly informed by our survey data through the specified likelihood.

Model calibration

To calibrate the model parameters, we ran independent DEzs-MCMCs on different training data sets: Five chains were run on the separate folds of the cross validation and one on the full data set. Differences between the respective sampled posterior distributions could therefore arise both because of differing convergence and because of the data selection. We found that all posteriors converged roughly in the same area of the parameter space, as the variance over the five folds was small. Their marginal distributions took on similar medians and quantiles.

A comparison between the prior and posterior distributions revealed how the consideration of the MHB survey data informed the initial parameter estimates obtained directly from literature data. Notably, the medians of the marginal distributions for fecundity ϕ_0 and the survival probabilities of the first and second stage σ_1 and σ_2 shifted significantly, whereas those of the other parameters remained largely unchanged. The marginal

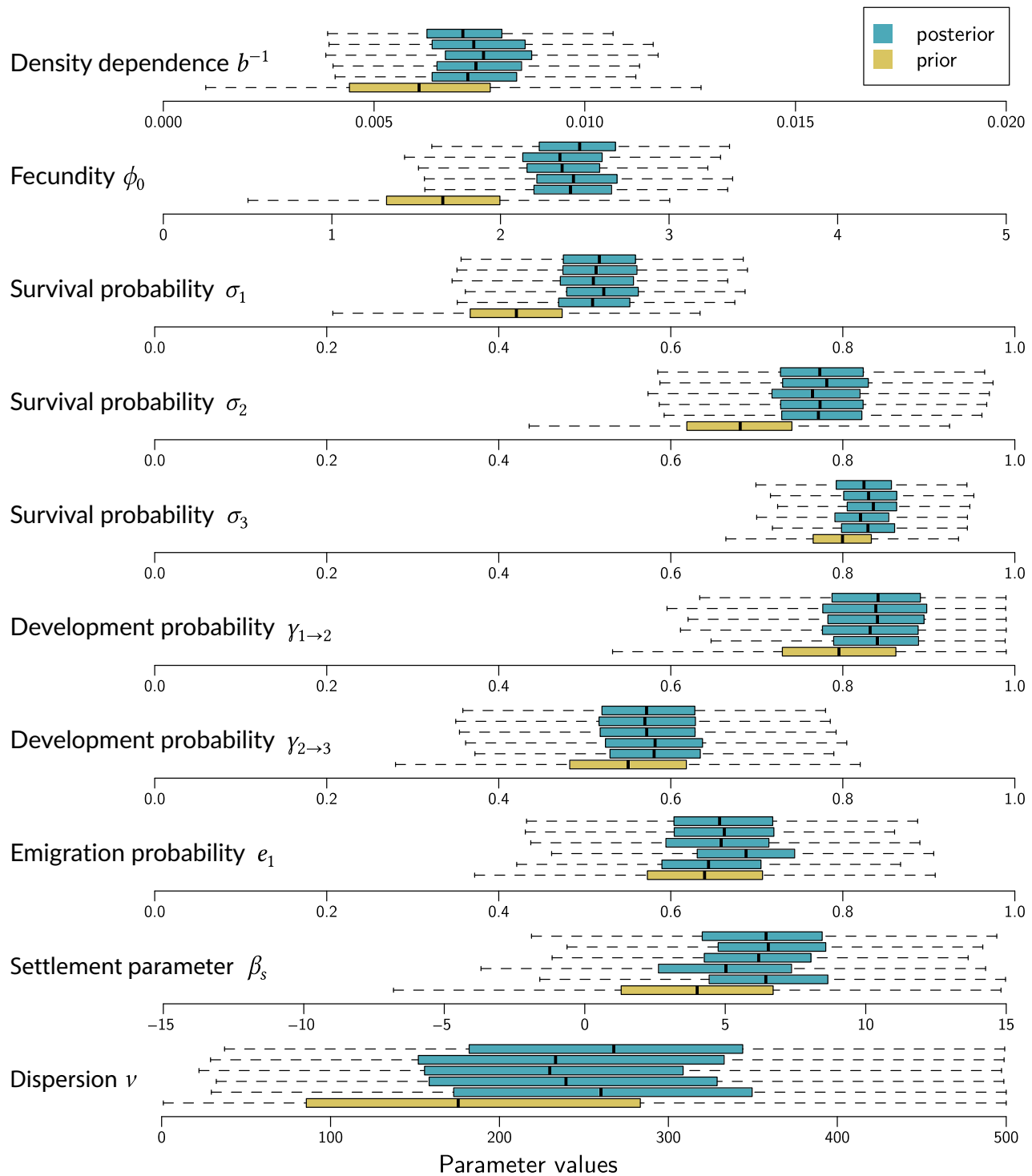


FIGURE 3 Box plots summarize the marginal prior (yellow) and posterior (blue) distribution for each calibration parameter and for all five spatial folds. The black bar marks the median, the boxes show the interquartile range, and the whiskers extend to the most extreme data point, which is no farther from the box than 1.5 times its length.

posterior distributions for each parameter and each spatial fold are represented by box plots in Figure 3, and those for the calibration to the full data set are shown in Appendix S1: Figure S12. Comparing the HPDIs of the prior and posterior distributions, we found substantially

narrower posteriors and, thus, reduced uncertainty for the strength of density dependence $1/b$, fecundity ϕ_0 , and the survival probabilities of stages one and two σ_1 and σ_2 . These parameters had already responded strongly in the sensitivity analysis. No uncertainty reduction or a

significant change in point estimate was found for adult survival σ_3 (Appendix S1: Figure S13). This was contrary to our expectation based on the sensitivity analysis, but this parameter already had the most informative priors to begin with. The dispersion parameter of the NB error model was calibrated to a very large value, yielding a variance that was close to that of a Poisson distribution. Thus, only slight overdispersion was detected relative to a Poisson-distributed error.

The convergence of all DEzs-MCMCs was regarded sufficient, based on the conducted diagnostics. However, there were considerable differences between the folds due to the varying number of MHB sites included: The chains reached multivariate PSRF values of 1.05, 1.02, 1.05, 1.09, and 1.04, respectively, for Folds 1 to 5. Convergence was further assessed using trace plots (Appendix S1: Figure S9), trace rank plots (Appendix S1: Figure S10), and PSRF plots (Appendix S1: Figure S11), which were all satisfactory. No substantial correlations between the parameters were detected (Appendix S1: Figure S14).

Model validation

The spatial-block cross-validation was evaluated by calculating the *c*-index per spatial fold and for different subsets of the MHB data (Table 2). First, it was calculated over all observations, that is, all site-year combinations within a fold, independently. The overall value of 0.88 indicates an excellent fit to the validation data. However, the results were quite variable across folds (see also Appendix S1: Figure S15), which is likely due to the

differing number and information content of the included MHB sites. Second, focusing on regional abundance dynamics, we calculated the *c*-index for the time series of the total abundance within each fold, consistently yielding excellent values between 0.92 and 0.94 (see also Appendix S1: Figure S16). This confirms that averaging the abundance over large regions further increased the accuracy of temporal predictions. Third, we were interested in the performance of our dSDMs at those MHB sites that showed the highest variance in red kite counts since highly fluctuating population sizes are often of special conservation interest but are usually harder to predict. To this end, we ranked all MHB sites by their count variance and computed the *c*-index over the top 15% most variable sites. The folds scored significantly lower, showing an overall value of 0.66 (see also Appendix S1: Figure S17), which signified a substantial drop in performance and indicated fair predictions for highly variable sites. Again, the different folds showed highly variable results that ranged from 0.59 to 0.75, depending on the specific sites they included.

Model projections

The model was used to generate projections to places not covered by the MHB survey by simulating red kite abundance over the whole extent of Switzerland. This made it possible to compare these projections to the Swiss breeding bird index, which estimates the total population trend relative to the year 1999 (Knaus et al., 2022) and, thus, offers an additional source of validation data. Further, by running the model forward beyond the MHB data period and under stable environmental conditions, we estimated the size and range of the current potential population.

Prior and posterior predictions of total red kite abundance during the entire survey period and 30 years onward, assuming constant habitat suitabilities, are shown in Figure 4. The posterior predictions showed very good fit to the Swiss breeding bird index. Comparison of the prior and posterior predictions of our model gave more evidence that the calibration was able to gain substantial information from the survey data: The model fit was improved considerably and output uncertainty was reduced. Simulations from the prior showed negative population trends in most cases, and they had a large 95% credibility interval that included predictions of five to 2100 BPs in year 2019. The posterior predictions, in contrast, showed increasing trends throughout and a much narrower credibility interval. They exhibited a comparably steep increase in abundance over the past 20 years, in accordance with the strong increases in red

TABLE 2 Evaluation of spatially blocked cross-validation (CV).

Spatial CV fold	Spatiotemporal	Temporal	High variance
Fold 1	0.69 (0.05)	0.94 (0.05)	0.67 (0.11)
Fold 2	0.86 (0.02)	0.93 (0.05)	0.59 (0.06)
Fold 3	0.89 (0.02)	0.94 (0.04)	0.65 (0.07)
Fold 4	0.92 (0.01)	0.92 (0.05)	0.75 (0.05)
Fold 5	0.85 (0.04)	0.92 (0.06)	0.73 (0.07)
All folds	0.88 (0.01)	0.94 (0.04)	0.66 (0.03)

Note: Each fold was used as test data for a separate calibration, which used the remaining folds as training data. Predictions to the test data were evaluated using the *c*-index, given per row by its mean and SD in brackets. The *c*-index was computed on different subsets of the MHB data, given per column: The spatiotemporal *c*-index compares each observation (site-year) independently, the temporal *c*-index compares time series of total abundance per fold, and the last column gives the *c*-index over sites with the 15% highest variance in local population size.

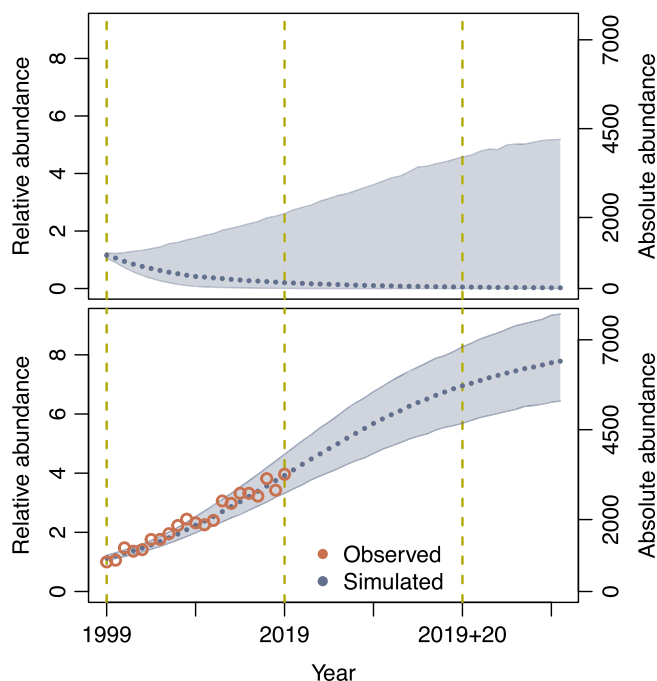


FIGURE 4 Prior (top) and posterior (bottom) simulations of abundance time series of red kite in Switzerland. The blue line and band show the median and 95% credibility interval of total number of predicted breeding pairs (number of BP), with relative values (with respect to year 1999) on the left-hand-side and absolute values on the right-hand-side y-axis. The bottom panel shows the cross-validated posterior predictions together with the breeding bird index (red circles, relative y-axis only) for comparison. The dashed vertical lines mark the years for which spatial projections are depicted in Figure 5. After 2019, the last year of survey data, the environmental conditions are kept constant.

kite abundance that were recorded during this time. Forward simulation showed that today's potential equilibrium population size amounts to 6400 (95% credibility interval: 5300–7700) BPs.

Spatial projections were made to the whole country as three snapshots in time (Figure 5): at the beginning (1999) and end (2019) of the survey data set and after a continuation of 20 more years (2019 + 20). These projections mirrored the rapid expansion of red kite range that Switzerland has seen in the past two decades. However, the continuation showed a relatively stable range with increasing population densities, suggesting that the current population has not yet reached the carrying capacity in all colonized areas. The same maps were created from prior predictions for comparison (Appendix S1: Figure S19). They exhibit a contracting range over time, which deviates substantially from the posterior maps, again indicating the effective inclusion of information from the MHB data.

This comparison of prior and posterior distributions and their respective predictions can shed light on the

main drivers of the presented results. While the prior predictions exhibited a tendency toward decreasing populations and contracting ranges, the posterior predictions reproduced the observed patterns closely. Comparison of the marginal distributions (Figure 3) revealed that the main drivers of these disparate predictions appeared to be fecundity and early survival rates. They responded most strongly to the information incorporated from the MHB data via the Bayesian calibration. Taken together, these three influential parameters suggest that reproductive success was determined to play a key role in driving the resulting increases in local density and distribution. In contrast, changes in habitat suitability over the study period seem to have had a lesser effect on the resulting population. This was assessed in a simple analysis of the sensitivity of simulated abundance to habitat suitability. We compared the abundance time series from Figure 4 with two counterfactual scenarios in which the habitat suitabilities of each year were raised or reduced by five (out of 100) habitat suitability points (Appendix S1: Figure S18). By the last year of MHB data, 2019, this intervention had an effect of 9%–10% on total abundance, which is small compared to the effect of the calibration (Figure 4). We thus concluded that the population increases were not predominantly driven by a changing environment but by transient dynamics of an equilibrium with much higher population size.

DISCUSSION

Reliable methodology for understanding and predicting a species' population and range dynamics will be crucial to inform decision making in the future. Dynamic, spatially explicit, process-based distribution models (dSDMs) provide valuable advances toward improved biodiversity forecasts (Urban et al., 2016) but are currently underused due to technical and data challenges and limited guidance for applications (Briscoe et al., 2019; Zurell et al., 2022). This study contributes to overcoming these challenges. We demonstrated the practicability of a complete modeling workflow for dSDMs with a case study of a conservation-relevant population, the red kite in Switzerland. This included calibrating a complex stochastic simulation model to heterogeneous empirical data, interpreting the results, and validating the model by cross-validation. Thanks to the use of Bayesian inference, we can integrate direct and indirect knowledge on the process parameters, account for their uncertainty, and propagate it to model projections. Our model captures the Swiss red kite population trends with higher spatial and temporal predictive accuracy than was achieved with correlative models in a previous study (details below;

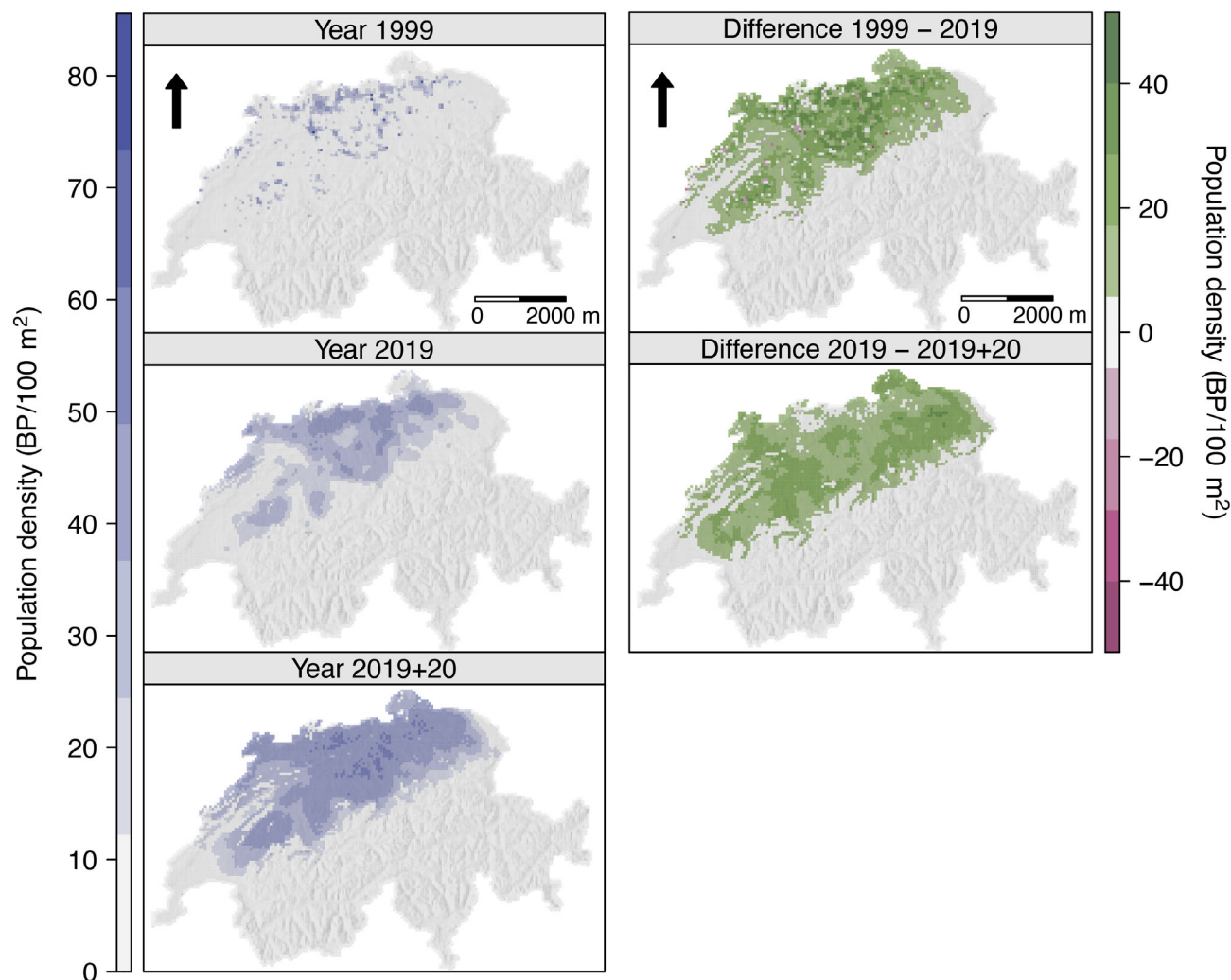


FIGURE 5 Mean posterior predicted population densities for years 1999 and 2019, and after 20 additional years under constant conditions (left column) as well as the differences between those years (right column). Arrows indicate north.

Briscoe et al., 2021). The model suggests that the potential population size under current environmental conditions is much larger than presently realized and that this may be a result of the population's history. The workflow exemplified here can be readily adapted to other species if an adequate model, prior parameter estimates, and response data (e.g., occupancy or abundance data) are available, and it promises to yield improved parameter estimates and more accurate, validated model projections.

The process-based dSDM used here to demonstrate our workflow was built with the individual-based modeling platform RangeShiftR (Malchow et al., 2021). It explicitly considers relevant ecological processes such as demography and dispersal and includes crucial mechanisms such as density dependence. Therefore, transient dynamics, which arise when a distribution is not in equilibrium with its environment, can be reproduced, and

dynamic responses to change can be represented. The IBM structure was determined based on expert opinion and the direct (prior) parameterizations of the process parameters were derived from literature data. IBM approaches are particularly suited for the direct estimation of their model parameters (e.g., survival probability or dispersal distance) because they formulate all processes from the perspective of the individual (Railsback & Grimm, 2019), where they can be estimated from data obtained in observational studies (e.g., mark-recapture). The prior estimates were updated using the MHB abundance data within a Bayesian inference. Here, IBMs have the advantage of realistically modeling small local populations of a few individuals by incorporating demographic stochasticity, so that the survey data can be used at a high spatial resolution. Depending on the research question and the available data, however, a different model formulation may be more adequate, such as

spatially explicit population-based models (implemented for example in the R package *steps*; Visintin et al., 2020). For a successful parameterization using the presented framework, certain data requirements should be met: The utilized model should have model parameters whose priors can be informed by ecological theory and direct estimates from field and experimental measurements, and it should generate outputs that can be compared to observational data via a plausible error model that can be expressed as a likelihood function.

The successful calibration of parameters in process-based dSDMs can produce new insights, since they have a well-defined ecological meaning. Comparing the prior and posterior distributions of our model, we found that some parameters in particular, for example, adult fecundity ϕ_0 , its density dependence $1/b$, and the survival probabilities of juveniles and subadults σ_1 and σ_2 , responded strongly to the inclusion of additional information from survey data. This behavior was predicted well by the local and global sensitivity analyses. The detected sensitivity further indicated that the model projections were responsive to these parameters, thereby suggesting potential pathways for conservation measures, for example, highlighting the protection of young individuals and supporting nest success. Pfeiffer and Schaub (2023) reached the same conclusion and identified the breeding output and adult survival as the main demographic drivers when modeling the German red kite population with an integrated population model. Further, their estimates of stage-wise survival probabilities are in strong agreement with ours. The prior estimate of $1/b$ was corroborated, and those of ϕ_0 , σ_1 , and σ_2 were corrected to higher values, while the uncertainty around all four estimates was reduced. These corrections in parameter distributions also drive the better fit of the calibrated model projections to the data as well as the reduced output uncertainty. Interestingly, it was shown that the calibration could acquire information even on the early developmental stages (1 and 2) that were not recorded in the calibration data, which held abundances of Stage 3 only. This was facilitated by the ecological assumptions that were imposed by the model structure, which discerned the stages by their ability to disperse (only Stage 1) or reproduce (only Stage 3).

The discrepancies found between prior and posterior parameter estimates are driven by different factors (Cailleret et al., 2020). First, there can be a true difference, for example, if the prior estimates had been obtained from different study populations. In our case, the prior fecundity was based on a measurement from a Swiss subpopulation with a high breeding density, which may have a lower fecundity than the Swiss average. The prior survival probabilities were taken from a German

red kite population that showed a slightly negative population trend, and the upward correction seemed to better match the increasing Swiss population. Red kite in Switzerland benefit from public feeding (Cereghetti et al., 2019), and many subadult individuals change from migratory to resident behavior, which can also increase survival. Second, an important source of deviations between empirical and calibrated parameter estimates is model error. Our IBM captured only a subset of the multiple eco-evolutionary processes that underlie the observed abundance patterns. Therefore, the calibrated parameters will account for missing processes to some extent. This highlights the need for further development of dSDMs to include more mechanisms and, thus, to fit observed data more closely. It further emphasizes the importance of effective integration of direct and inverse calibration to estimate parameter values and their uncertainties, since projections and derived management decisions can be highly sensitive to the final parameterization.

The validation of model predictions to assess model performance is common practice in the application of cSDMs (Sillero et al., 2021) but is often missing with dSDMs. With the presented workflow, we successfully applied spatial-block cross-validation to a dSDM by calibrating the model to each of five spatially contiguous regions within the study area. By spatially blocking the holdout data, we reduced the amount of spatial autocorrelation between the training and testing data, which is often present in abundance data and only insufficiently reduced by other cross-validation schemes such as randomized leave-p-out. This yields a more realistic assessment of predictive performance for interpolation. For other types of data, different blocking techniques may be more adequate (Roberts et al., 2017). The folds were selected carefully in such a way that the same range of environmental conditions was represented in each one, so that model evaluation did not involve extrapolation to new environmental conditions. Performing a cross-validation is usually computationally expensive, as the calibration needs to be repeated for each set of holdout data. Therefore, a suitable validation method must be chosen carefully. Alternatives include approximation to leave-one-out validation by Watanabe-Akaike information criterion (Vehtari et al., 2017).

The full red kite dSDM was evaluated based on its cross-validated abundance predictions using Harrell's *c*-index as a measure of predictive performance, which indicated excellent predictive accuracy (*c*-index: 0.88). In sites with highly fluctuating abundances, performance dropped considerably and only yielded fair predictions (*c*-index: 0.66). A similar analysis was conducted by Briscoe et al. (2021), who compared the accuracy of correlative

SDMs and dynamic occupancy models (Kéry et al., 2013) that were fitted to the MHB data of 69 Swiss birds, including the red kite. They found that the predictive ability of occupancy was high for all examined model types when assessed across all sites (mean AUC >0.8) but much lower when specifically testing only sites that showed occupancy change (mean AUC 0.64–0.71). The AUC metric is based on predictions of occupancy only and therefore generally scores above the *c*-index, which ranks abundances. In collapsing our abundance predictions to occupancy and comparing them to Briscoe et al. (2021) in terms of the AUC, our calibrated IBM surpasses the mean of their red kite SDMs, across both all sites (mean AUC of 0.91 vs. 0.85) and occupancy-switching sites only (0.80 vs. 0.67). Especially in range-shifting populations, such as the red kite in Switzerland, process-explicit dSDMs can outperform correlative approaches because they make no equilibrium assumption. Our model also showed clear advantages over the dynamic occupancy models in Briscoe et al. (2021), likely due to the explicit consideration of spatially explicit processes such as density dependence in population dynamics and dispersal.

The calibrated model was run forward under current environmental conditions in order to explore the potential population size and distribution. In the same way, it could be used to assess population trends under certain scenarios such as conservation measures involving habitat improvements or regulation of demographic rates. For predictions of future population dynamics, however, expected changes in land use and climate must be taken into account. In our dSDM, these variables are only considered through the cSDM-derived, scalar habitat suitability and thus cannot impact demographic processes directly and independently, as ecological theory suggests. More complexity and mechanistic understanding could be incorporated by substituting the habitat model with direct relationships of species traits like demographic rates with environmental variables. Such a demographic range model is adequate for predictions under climate change (Malchow, Hartig, et al., 2023; Schurr et al., 2012). As a further limitation, the habitat map that underlies our model consists of a cSDM fitted to recent atlas data. It is possible that suitable but not yet occupied parts of the red kite niche were missed in these data, so the future range would be underestimated by the projections. This limitation can be circumvented by using a habitat model that does not rely on the equilibrium assumption, for example, a rule-based model derived from knowledge about the species' habitat requirements or an eco-physiological SDM (Kearney & Porter, 2009). Moreover, the observed increases in range and density might have been partially fueled by individuals that had not been recruited in the study region but immigrated

from surrounding high-density populations that were not considered in the model. More potential for model improvement lies in implementing additional processes such as mating systems, species interactions, or genetic and behavioral adaptation. Their successful parameterization, however, will require adequate data.

The inverse calibration of dSDMs from observational data is also possible with other methods, like pattern-oriented modeling (Grimm et al., 2005; Mortensen et al., 2021) or approximate Bayesian computation (Beaumont, 2010; Hauenstein et al., 2019), the latter of which has already been demonstrated in the RangeShifter model (Dominguez Almela et al., 2020). Independently of the chosen calibration method, the accurate parameterization of dynamic and mechanistic SDMs will remain a challenge until the paucity of high-quality ecological and monitoring data is alleviated (Kissling et al., 2018; Oliver et al., 2012). Which parameters of a dSDM can be successfully calibrated depends on the available calibration data. Here, the type of data collected within monitoring programs plays an important role as all model output quantities can principally be used for inverse parameterization. In our case study, for example, the abundances of juveniles and subadults were output from the IBM but could not be used for calibration because age classes are not distinguished in MHB surveys. Generally, the considerable uncertainties in parameter estimates caused by data limitations translate to large credibility intervals in model projections, reducing the utility for conservation applications. Here, it is a clear advantage of the Bayesian framework that sources of outcome uncertainty are explicitly quantified and can thus be addressed, for example, in targeted monitoring programs.

In conclusion, this case study shows how an individual-based dSDM can be built with RangeShiftR, calibrated using Bayesian inference, and validated by cross-validation. We demonstrated how the inclusion of monitoring data refined parameter estimates and greatly improved model fit and prediction accuracy, thereby offering improved insights into underlying mechanisms. Well-calibrated and validated process-based models offer compelling advantages over the currently most common static models. They are able to inform science-based management decisions and the design of proactive conservation measures (Zurell et al., 2022). Future progress in this field should be directed toward developing more flexible and accessible modeling tools, assessing their data requirements for effective parameterization, and validating them against independent targets.

AUTHOR CONTRIBUTIONS

Anne-Kathleen Malchow: Conceptualization (equal), formal analysis (lead), methodology (equal), software (lead),

data curation (equal), visualization (lead), writing—original draft preparation (lead), writing—review and editing (equal). Guillermo Fandos: Conceptualization (equal), methodology (equal), writing—review and editing (equal). Urs G. Kormann: Conceptualization (equal), data curation (equal), methodology (equal), writing—review and editing (equal). Martin U. Grüebler: Conceptualization (equal), data curation (equal), methodology (equal), writing—review and editing (equal). Marc Kéry: Conceptualization (equal), data curation (equal), writing—review and editing (equal). Florian Hartig: Conceptualization (equal), formal analysis (support), methodology (equal), supervision (support), writing—review and editing (equal). Damaris Zurell: Conceptualization (equal), methodology (equal), funding acquisition (lead), supervision (lead), writing—review and editing (equal).

ACKNOWLEDGMENTS

Anne-Kathleen Malchow and Damaris Zurell were supported by Deutsche Forschungsgemeinschaft under Grant agreement ZU 361/1-1. This publication has been prepared using European Union's Copernicus Land Monitoring Service information. Open Access funding enabled and organized by Projekt DEAL.

CONFLICT OF INTEREST STATEMENT

The authors declare no conflicts of interest.

DATA AVAILABILITY STATEMENT


Data and code (Malchow, Fandos, et al., 2023) to replicate the presented analyses are available in Zenodo at <https://doi.org/10.5281/zenodo.10435418>. A development version of the R package RangeShiftR was used and is available in Malchow et al. (2022) in Zenodo at <https://doi.org/10.5281/zenodo.10689677>.

ORCID

Anne-Kathleen Malchow  <https://orcid.org/0000-0003-1446-6365>

Guillermo Fandos  <https://orcid.org/0000-0003-1579-9444>

Urs G. Kormann  <https://orcid.org/0000-0001-9875-4836>

Martin U. Grüebler  <https://orcid.org/0000-0003-4468-8292>

Marc Kéry  <https://orcid.org/0000-0001-7476-7616>

Florian Hartig  <https://orcid.org/0000-0002-6255-9059>

Damaris Zurell  <https://orcid.org/0000-0002-4628-3558>

REFERENCES

- Aebischer, A., and P. Scherler. 2021. *Der Rotmilan—Ein Greifvogel im Aufwind*, 1st ed. 232. Bern: Haupt Verlag.
- Andrieu, C., and G. O. Roberts. 2009. "The Pseudo-Marginal Approach for Efficient Monte Carlo Computations." *The Annals of Statistics* 37(2): 697–725. <https://doi.org/10.1214/07-AOS574>.
- Araújo, M. B., and A. T. Peterson. 2012. "Uses and Misuses of Bioclimatic Envelope Modeling." *Ecology* 93(7): 1527–39. <https://doi.org/10.1890/11-1930.1>.
- Arlot, S., and A. Celisse. 2010. "A Survey of Cross-Validation Procedures for Model Selection." *Statistics Surveys* 4: 40–79. <https://doi.org/10.1214/09-SS054>.
- Barber-O'Malley, B., G. Lassalle, G. Chust, E. Diaz, A. O'Malley, C. Paradinas Blázquez, J. Pórtoles Marquina, and P. Lambert. 2022. "HyDiaD: A Hybrid Species Distribution Model Combining Dispersal, Multi-Habitat Suitability, and Population Dynamics for Diadromous Species under Climate Change Scenarios." *Ecological Modelling* 470: 109997. <https://doi.org/10.1016/j.ecolmodel.2022.109997>.
- Bauks, C. 2018. "The Effect of Food Supplementation on Range Use of Breeding Red Kites (*Milvus milvus*) in Switzerland." Master thesis, Swiss Ornithological Institute Sempach.
- Beaumont, M. A. 2010. "Approximate Bayesian Computation in Evolution and Ecology." *Annual Review of Ecology, Evolution, and Systematics* 41(1): 379–406. <https://doi.org/10.1146/annurev-ecolsys-102209-144621>.
- Bleyhl, B., A. Ghoddousi, E. Askerov, G. Bocedi, U. Breitenmoser, K. Manvelyan, S. C. F. Palmer, et al. 2021. "Reducing Persecution Is more Effective for Restoring Large Carnivores than Restoring their Prey." *Ecological Applications* 31(5): e02338. <https://doi.org/10.1002/eap.2338>.
- Bocedi, G., S. C. F. Palmer, A.-K. Malchow, D. Zurell, K. Watts, and J. M. J. Travis. 2021. "RangeShifter 2.0: An Extended and Enhanced Platform for Modelling Spatial Eco-Evolutionary Dynamics and species' Responses to Environmental Changes." *Ecography* 44(10): 1453–62. <https://doi.org/10.1111/ecog.05687>.
- Bolam, F. C., L. Mair, M. Angelico, T. M. Brooks, M. Burgman, C. Hermes, M. Hoffmann, et al. 2021. "How Many Bird and Mammal Extinctions Has Recent Conservation Action Prevented?" *Conservation Letters* 14(1): e12762. <https://doi.org/10.1111/conl.12762>.
- Briscoe, N. J., J. Elith, R. Salguero-Gómez, J. J. Lahoz-Monfort, J. S. Camac, K. M. Giljohann, M. H. Holden, et al. 2019. "Forecasting Species Range Dynamics with Process-Explicit Models: Matching Methods to Applications." *Ecology Letters* 22(11): 1940–56. <https://doi.org/10.1111/ele.13348>.
- Briscoe, N. J., D. Zurell, J. Elith, C. König, G. Fandos, A.-K. Malchow, M. Kéry, H. Schmid, and G. Guillera-Aroita. 2021. "Can Dynamic Occupancy Models Improve Predictions of Species' Range Dynamics? A Test Using Swiss Birds." *Global Change Biology* 27(18): 4269–82. <https://doi.org/10.1111/gcb.15723>.
- Broms, K. M., M. B. Hooten, D. S. Johnson, R. Altwegg, and L. L. Conquest. 2016. "Dynamic Occupancy Models for Explicit Colonization Processes." *Ecology* 97(1): 194–204. <https://doi.org/10.1890/15-0416.1>.
- Cailleret, M., N. Bircher, F. Hartig, L. Hülsmann, and H. Bugmann. 2020. "Bayesian Calibration of a Growth-Dependent Tree Mortality Model to Simulate the Dynamics of European Temperate Forests." *Ecological Applications* 30(1): e02021. <https://doi.org/10.1002/eap.2021>.
- Cereghetti, E., P. Scherler, J. Fattebert, and M. U. Grüebler. 2019. "Quantification of Anthropogenic Food Subsidies to an Avian Facultative Scavenger in Urban and Rural Habitats."

- Landscape and Urban Planning* 190: 103606. <https://doi.org/10.1016/j.landurbplan.2019.103606>.
- Copernicus Land Monitoring Service. 2022. *Corine Land Cover Data set*. European Environment Agency, Copenhagen, Denmark. URL: <http://data.europa.eu/88u/dataset/DAT-195-en>
- Csilléry, K., O. François, and M. G. Blum. 2012. “abc: An R Package for Approximate Bayesian Computation (ABC).” *Methods in Ecology and Evolution* 3(3): 475–79.
- DeAngelis, D. L., and W. M. Mooij. 2005. “Individual-Based Modeling of Ecological and Evolutionary Processes.” *Annual Review of Ecology, Evolution, and Systematics* 36(1): 147–168. <https://doi.org/10.1146/annurev.ecolsys.36.102003.152644>.
- Díaz, S., J. Settele, E. S. Brondízio, H. T. Ngo, J. Agard, A. Arneeth, P. Balvanera, et al. 2019. “Pervasive Human-Driven Decline of Life on Earth Points to the Need for Transformative Change.” *Science* 366(6471): eaax3100. <https://doi.org/10.1126/science.aax3100>.
- Dominguez Almela, V., S. C. F. Palmer, P. K. Gillingham, J. M. J. Travis, and J. R. Britton. 2020. “Integrating an Individual-Based Model with Approximate Bayesian Computation to Predict the Invasion of a Freshwater Fish Provides Insights into Dispersal and Range Expansion Dynamics.” *Biological Invasions* 22(4): 1461–80. <https://doi.org/10.1007/s10530-020-02197-6>.
- Dormann, C. F., J. Elith, S. Bacher, C. Buchmann, G. Carl, G. Carré, J. R. G. Marquéz, et al. 2013. “Collinearity: A Review of Methods to Deal with it and a Simulation Study Evaluating their Performance.” *Ecography* 36(1): 27–46. <https://doi.org/10.1111/j.1600-0587.2012.07348.x>.
- Dormann, C. F., S. J. Schymanski, J. Cabral, I. Chuine, C. Graham, F. Hartig, M. Kearney, et al. 2012. “Correlation and Process in Species Distribution Models: Bridging a Dichotomy.” *Journal of Biogeography* 39(12): 2119–31. <https://doi.org/10.1111/j.1365-2699.2011.02659.x>.
- Dormann, C. F., J. M. McPherson, M. B. Araújo, R. Bivand, J. Bolliger, G. Carl, R. G. Davies, et al. 2007. “Methods to Account for Spatial Autocorrelation in the Analysis of Species Distributional Data: A Review.” *Ecography* 30(5): 609–628. <https://doi.org/10.1111/j.2007.0906-7590.05171.x>.
- Duarte, C. M., S. Agusti, E. Barbier, G. L. Britten, J. C. Castilla, J.-P. Gattuso, R. W. Fulweiler, et al. 2020. “Rebuilding Marine Life.” *Nature* 580(7801): 39–51. <https://doi.org/10.1038/s41586-020-2146-7>.
- Elith, J., and J. R. Leathwick. 2009. “Species Distribution Models: Ecological Explanation and Prediction across Space and Time.” *Annual Review of Ecology, Evolution, and Systematics* 40(1): 677–697. <https://doi.org/10.1146/annurev.ecolsys.110308.120159>.
- Fordham, D. A., S. Haythorne, S. C. Brown, J. C. Buettel, and B. W. Brook. 2021. “poems: R Package for Simulating Species’ Range Dynamics Using Pattern-Oriented Validation.” *Methods in Ecology and Evolution* 12(12): 2364–71. <https://doi.org/10.1111/2041-210X.13720>.
- Franklin, J. 2013. “Species Distribution Models in Conservation Biogeography: Developments and Challenges.” *Diversity and Distributions* 19(10): 1217–23. <https://doi.org/10.1111/ddi.12125>.
- Gallien, L., T. Münkemüller, C. H. Albert, I. Boulangeat, and W. Thuiller. 2010. “Predicting Potential Distributions of Invasive Species: Where to Go from Here?” *Diversity and Distributions* 16(3): 331–342. <https://doi.org/10.1111/j.1472-4642.2010.00652.x>.
- Gelman, A., and D. B. Rubin. 1992. “Inference from Iterative Simulation Using Multiple Sequences.” *Statistical Science* 7(4): 457–472. <https://doi.org/10.1214/ss/1177011136>.
- Grimm, V., S. F. Railsback, C. E. Vincenot, U. Berger, C. Gallagher, D. L. DeAngelis, B. Edmonds, et al. 2020. “The ODD Protocol for Describing Agent-Based and Other Simulation Models: A Second Update to Improve Clarity, Replication, and Structural Realism.” *Journal of Artificial Societies and Social Simulation* 23: 2.
- Grimm, V., E. Revilla, U. Berger, F. Jeltsch, W. M. Mooij, S. F. Railsback, H.-H. Thulke, J. Weiner, T. Wiegand, and D. L. DeAngelis. 2005. “Pattern-Oriented Modeling of Agent-Based Complex Systems: Lessons from Ecology.” *Science* 310(5750): 987–991. <https://doi.org/10.1126/science.1116681>.
- Guisan, A., and W. Thuiller. 2005. “Predicting Species Distribution: Offering More than Simple Habitat Models.” *Ecology Letters* 8(9): 993–1009. <https://doi.org/10.1111/j.1461-0248.2005.00792.x>.
- Guisan, A., R. Tingley, J. B. Baumgartner, I. Naujokaitis-Lewis, P. R. Sutcliffe, A. I. T. Tulloch, T. J. Regan, et al. 2013. “Predicting Species Distributions for Conservation Decisions.” *Ecology Letters* 16(12): 1424–35. <https://doi.org/10.1111/ele.12189>.
- Hagen, O., B. Flück, F. Fopp, J. S. Cabral, F. Hartig, M. Pontarp, T. F. Rangel, and L. Pellissier. 2021. “gen3sis: A General Engine for Eco-Evolutionary Simulations of the Processes that Shape Earth’s Biodiversity.” *PLoS Biology* 19(7): e3001340. <https://doi.org/10.1371/journal.pbio.3001340>.
- Hartig, F., J. Dyke, T. Hickler, S. I. Higgins, R. B. O’Hara, S. Scheiter, and A. Huth. 2012. “Connecting Dynamic Vegetation Models to Data—An Inverse Perspective.” *Journal of Biogeography* 39(12): 2240–52. <https://doi.org/10.1111/j.1365-2699.2012.02745.x>.
- Hartig, F., F. Minunno, and S. Paul. 2019. “BayesianTools: General-Purpose MCMC and SMC Samplers and Tools for Bayesian Statistics.” R Package Version 0.1.7.
- Hauenstein, S., J. Fattebert, M. U. Gruebler, B. Naef-Daenzer, G. Pe’er, and F. Hartig. 2019. “Calibrating an Individual-Based Movement Model to Predict Functional Connectivity for Little Owls.” *Ecological Applications* 29(4): e01873. <https://doi.org/10.1002/eap.1873>.
- Hefley, T. J., M. B. Hooten, R. E. Russell, D. P. Walsh, and J. A. Powell. 2017. “When Mechanism Matters: Bayesian Forecasting Using Models of Ecological Diffusion.” *Ecology Letters* 20(5): 640–650.
- Hobbs, N. T., and M. B. Hooten. 2015. *Bayesian Models: A Statistical Primer for Ecologists*. Princeton, NJ: Princeton University Press.
- Hoffmann, M., C. Hilton-Taylor, A. Angulo, M. Böhm, T. M. Brooks, S. H. M. Butchart, K. E. Carpenter, et al. 2010. “The Impact of Conservation on the Status of the World’s Vertebrates.” *Science* 330(6010): 1503–9. <https://doi.org/10.1126/science.1194442>.
- Jaatinen, K., M. Westerborn, A. Norkko, O. Mustonen, and D. N. Koons. 2021. “Detrimental Impacts of Climate Change May be Exacerbated by Density-Dependent Population Regulation in

- Blue Mussels." *Journal of Animal Ecology* 90(3): 562–573. <https://doi.org/10.1111/1365-2656.13377>.
- Karger, D. N. 2018. "Data from: Climatologies at High Resolution for the Earth's Land Surface Areas." Dryad. <https://doi.org/10.5061/dryad.kd1d4>.
- Karger, D. N., O. Conrad, J. Böhner, T. Kawohl, H. Kreft, R. W. Soria-Auza, N. E. Zimmermann, H. P. Linder, and M. Kessler. 2017. "Climatologies at High Resolution for the Earth's Land Surface Areas." *Scientific Data* 4: 170122. <https://doi.org/10.1038/sdata.2017.122>.
- Katzenberger, J., E. Gottschalk, N. Balkenhol, and M. Waltert. 2019. "Long-Term Decline of Juvenile Survival in German Red Kites." *Journal of Ornithology* 160(2): 337–349. <https://doi.org/10.1007/s10336-018-1619-z>.
- Kearney, M., and W. Porter. 2009. "Mechanistic Niche Modelling: Combining Physiological and Spatial Data to Predict Species' Ranges." *Ecology Letters* 12(4): 334–350. <https://doi.org/10.1111/j.1461-0248.2008.01277.x>.
- Keith, D. A., H. R. Akçakaya, W. Thuiller, G. F. Midgley, R. G. Pearson, S. J. Phillips, H. M. Regan, M. B. Araújo, and T. G. Rebelo. 2008. "Predicting Extinction Risks under Climate Change: Coupling Stochastic Population Models with Dynamic Bioclimatic Habitat Models." *Biology Letters* 4(5): 560–63. <https://doi.org/10.1098/rsbl.2008.0049>.
- Kéry, M., G. Guillera-Aroita, and J. J. Lahoz-Monfort. 2013. "Analysing and Mapping Species Range Dynamics Using Occupancy Models." *Journal of Biogeography* 40(8): 1463–74. <https://doi.org/10.1111/jbi.12087>.
- Kissling, W. D., J. A. Ahumada, A. Bowser, M. Fernandez, N. Fernández, E. A. García, R. P. Guralnick, et al. 2018. "Building Essential Biodiversity Variables (EBVs) of Species Distribution and Abundance at a Global Scale." *Biological Reviews* 93(1): 600–625. <https://doi.org/10.1111/brv.12359>.
- Knaus, P., G. Jérôme, T. Sattler, S. Wechsler, M. Kéry, N. Strebel, and S. Antoniazza. 2018. *Schweizer Brutvogelatlas 2013–2016*. Sempach: Schweizerische Vogelwarte.
- Knaus, P., N. Strebel, and T. Sattler. 2022. *The State of Birds in Switzerland 2022*. Sempach: Swiss Ornithological Institute.
- Landguth, E. L., A. Bearlin, C. C. Day, and J. Dunham. 2017. "CDMetaPOP: An Individual-Based, Eco-Evolutionary Model for Spatially Explicit Simulation of Landscape Demogenetics." *Methods in Ecology and Evolution* 8(1): 4–11. <https://doi.org/10.1111/2041-210X.12608>.
- Luengo, D., L. Martino, M. Bugallo, V. Elvira, and S. Särkkä. 2020. "A Survey of Monte Carlo Methods for Parameter Estimation." *EURASIP Journal on Advances in Signal Processing* 2020(1): 25. <https://doi.org/10.1186/s13634-020-00675-6>.
- Malchow, A.-K., G. Bocedi, S. C. F. Palmer, J. M. J. Travis, and D. Zurell. 2021. "RangeShiftR: An R Package for Individual-Based Simulation of Spatial Eco-Evolutionary Dynamics and species' Responses to Environmental Changes." *Ecography* 44(10): 1443–52. <https://doi.org/10.1111/ecog.05689>.
- Malchow, A.-K., G. Fandos, U. G. Kormann, M. U. Gruebler, M. Kéry, F. Hartig, and D. Zurell. 2023. "Fitting Individual-Based Models of Spatial Population Dynamics to Long-Term Monitoring Data." Zenodo. <https://doi.org/10.5281/zenodo.10435418>.
- Malchow, A.-K., F. Hartig, J. Reeg, M. Kéry, and D. Zurell. 2023. "Demography-Environment Relationships Improve Mechanistic Understanding of Range Dynamics under Climate Change." *Philosophical Transactions of the Royal Society B* 378: 20220194. <https://doi.org/10.1098/rstb.2022.0194>.
- Malchow, A.-K., J. Reeg, and D. Zurell. 2022. "RangeShiftR v.1.1-beta.0 (v.1.1-beta.0)." Zenodo. <https://doi.org/10.5281/zenodo.10689677>.
- Marion, G., G. J. McInerny, J. Pagel, S. Catterall, A. R. Cook, F. Hartig, and R. B. O'Hara. 2012. "Parameter and Uncertainty Estimation for Process-Oriented Population and Distribution Models: Data, Statistics and the Niche." *Journal of Biogeography* 39(12): 2225–39. <https://doi.org/10.1111/j.1365-2699.2012.02772.x>.
- Morris, M. D. 1991. "Factorial Sampling Plans for Preliminary Computational Experiments." *Technometrics* 33(2): 161–174. <https://doi.org/10.1080/00401706.1991.10484804>.
- Mortensen, L. O., M. E. Chudzinska, H. Slabbekoorn, and F. Thomsen. 2021. "Agent-Based Models to Investigate Sound Impact on Marine Animals: Bridging the Gap between Effects on Individual Behaviour and Population Level Consequences." *Oikos* 130(7): 1074–86. <https://doi.org/10.1111/oik.08078>.
- Moulin, T., A. Perasso, P. Calanca, and F. Gillet. 2021. "DynaGraM: A Process-Based Model to Simulate Multi-Species Plant Community Dynamics in Managed Grasslands." *Ecological Modelling* 439: 109345. <https://doi.org/10.1016/j.ecolmodel.2020.109345>.
- Nachtigall, W. 2008. *Der Rotmilan (Milvus milvus, L. 1758) in Sachsen und Südbrandenburg—Untersuchungen zu Verbreitung und Ökologie*. PhD diss., Universitäts- und Landesbibliothek Sachsen-Anhalt.
- Nägeli, M., P. Scherler, S. Witzak, B. Catitti, A. Aebischer, V. van Bergen, U. Kormann, and M. U. Gruebler. 2021. "Weather and Food Availability Additively Affect Reproductive Output in an Expanding Raptor Population." *Oecologia* 198: 125–138. <https://doi.org/10.1007/s00442-021-05076-6>.
- Newbold, T., L. N. Hudson, S. L. L. Hill, S. Contu, I. Lysenko, R. A. Senior, L. Börger, et al. 2015. "Global Effects of Land Use on Local Terrestrial Biodiversity." *Nature* 520(7545): 45–50. <https://doi.org/10.1038/nature14324>.
- Newson, R. 2006. "Confidence Intervals for Rank Statistics: Somers' D and Extensions." *The Stata Journal* 6(3): 309–334. <https://doi.org/10.1177/1536867X0600600302>.
- Newton, I., P. Davis, and J. Davis. 1989. "Age of First Breeding, Dispersal and Survival of Red Kites *Milvus milvus* in Wales." *Ibis* 131(1): 16–21.
- Oliver, T. H., S. Gillings, M. Girardello, G. Rapacciuolo, T. M. Brereton, G. M. Siriwardena, D. B. Roy, R. Pywell, and R. J. Fuller. 2012. "Population Density but Not Stability Can be Predicted from Species Distribution Models." *Journal of Applied Ecology* 49(3): 581–590. <https://doi.org/10.1111/j.1365-2664.2012.02138.x>.
- Pellissier, L., R. P. Rohr, C. Ndiribe, J.-N. Pradervand, N. Salamin, A. Guisan, and M. Wisz. 2013. "Combining Food Web and Species Distribution Models for Improved Community Projections." *Ecology and Evolution* 3(13): 4572–83. <https://doi.org/10.1002/ece3.843>.
- Pfeiffer, T., and M. Schaub. 2023. "Productivity Drives the Dynamics of a Red Kite Source Population that Depends on Immigration." *Journal of Avian Biology* 2023(1–2): e02984.

- R Core Team. 2020. *R: A Language and Environment for Statistical Computing*. Vienna: R Foundation for Statistical Computing.
- Railsback, S. F., and V. Grimm. 2019. *Agent-Based and Individual-Based Modeling: A Practical Introduction*, Second ed. 359. Princeton, NJ: Princeton University Press.
- Risk, B. B., P. de Valpine, and S. R. Beissinger. 2011. "A Robust-Design Formulation of the Incidence Function Model of Metapopulation Dynamics Applied to Two Species of Rails." *Ecology* 92(2): 462–474. <https://doi.org/10.1890/09-2402.1>.
- Roberts, D. R., V. Bahn, S. Ciuti, M. S. Boyce, J. Elith, G. Guillera-Arroita, S. Hauenstein, et al. 2017. "Cross-Validation Strategies for Data with Temporal, Spatial, Hierarchical, or Phylogenetic Structure." *Ecography* 40(8): 913–929. <https://doi.org/10.1111/ecog.02881>.
- Rodríguez, L., J. J. García, F. Carreño, and B. Martínez. 2019. "Integration of Physiological Knowledge into Hybrid Species Distribution Modelling to Improve Forecast of Distributional Shifts of Tropical Corals." *Diversity and Distributions* 25(5): 715–728. <https://doi.org/10.1111/ddi.12883>.
- Santos, E. P., H. H. Wagner, S. F. B. Ferraz, and T. Siqueira. 2020. "Interactive Persistent Effects of Past Land-Cover and its Trajectory on Tropical Freshwater Biodiversity." *Journal of Applied Ecology* 57(11): 2149–58. <https://doi.org/10.1111/1365-2664.13717>.
- Schaub, M. 2012. "Spatial Distribution of Wind Turbines Is Crucial for the Survival of Red Kite Populations." *Biological Conservation* 155: 111–18. <https://doi.org/10.1016/j.biocon.2012.06.021>.
- Schmid, H., R. Luder, B. Naef-Daenzer, R. Graf, and N. Zbinden. 1998. *Schweizer Brutvogelatlas 1993–1996*. Sempach: Schweizerische Vogelwarte.
- Schmid, H., N. Zbinden, and V. Keller. 2004. *Überwachung der Bestandsentwicklung Häufiger Brutvögel in der Schweiz*. Sempach: Schweizerische Vogelwarte.
- Schmolke, A., P. Thorbek, D. L. DeAngelis, and V. Grimm. 2010. "Ecological Models Supporting Environmental Decision Making: A Strategy for the Future." *Trends in Ecology & Evolution* 25(8): 479–486. <https://doi.org/10.1016/j.tree.2010.05.001>.
- Schurr, F. M., J. Pagel, J. S. Cabral, J. Groeneveld, O. Bykova, R. B. O'Hara, F. Hartig, et al. 2012. "How to Understand Species' Niches and Range Dynamics: A Demographic Research Agenda for Biogeography." *Journal of Biogeography* 39(12): 2146–62. <https://doi.org/10.1111/j.1365-2699.2012.02737.x>.
- Schweiger, O., R. K. Heikkinen, A. Harpke, T. Hickler, S. Klotz, O. Kudrna, I. Kühn, J. Pöyry, and J. Settele. 2012. "Increasing Range Mismatching of Interacting Species under Global Change Is Related to their Ecological Characteristics." *Global Ecology and Biogeography* 21(1): 88–99. <https://doi.org/10.1111/j.1466-8238.2010.00607.x>.
- Selwood, K. E., M. A. McGeoch, and R. Mac Nally. 2015. "The Effects of Climate Change and Land-Use Change on Demographic Rates and Population Viability." *Biological Reviews* 90(3): 837–853. <https://doi.org/10.1111/brv.12136>.
- Semper-Pascual, A., C. Burton, M. Baumann, J. Decarre, G. Gavier-Pizarro, B. Gómez-Valencia, L. Macchi, et al. 2021. "How Do Habitat Amount and Habitat Fragmentation Drive Time-Delayed Responses of Biodiversity to Land-Use Change?" *Proceedings of the Royal Society B: Biological Sciences* 288(1942): 20202466. <https://doi.org/10.1098/rspb.2020.2466>.
- Sergio, F., G. Tavecchia, J. Blas, A. Tanferna, and F. Hiraldo. 2021. "Demographic Modeling to Fine-Tune Conservation Targets: Importance of Pre-Adults for the Decline of an Endangered Raptor." *Ecological Applications* 31(3): e2266. <https://doi.org/10.1002/eap.2266>.
- Sillero, N., S. Arenas-Castro, U. Enriquez-Urzelai, C. G. Vale, D. Sousa-Guedes, F. Martínez-Freiría, R. Real, and A. M. Barbosa. 2021. "Want to Model a Species Niche? A Step-by-Step Guideline on Correlative Ecological Niche Modelling." *Ecological Modelling* 456: 109671. <https://doi.org/10.1016/j.ecolmodel.2021.109671>.
- Singer, A., O. Schweiger, I. Kühn, and K. Johst. 2018. "Constructing a Hybrid Species Distribution Model from Standard Large-Scale Distribution Data." *Ecological Modelling* 373: 39–52. <https://doi.org/10.1016/j.ecolmodel.2018.02.002>.
- Smolik, M., S. Dullinger, F. Essl, I. Kleinbauer, M. Leitner, J. Peterseil, L.-M. Stadler, and G. Vogl. 2010. "Integrating Species Distribution Models and Interacting Particle Systems to Predict the Spread of an Invasive Alien Plant." *Journal of Biogeography* 37(3): 411–422. <https://doi.org/10.1111/j.1365-2699.2009.02227.x>.
- ter Braak, C. J. F., and J. A. Vrugt. 2008. "Differential Evolution Markov Chain with Snooker Updater and Fewer Chains." *Statistics and Computing* 18(4): 435–446. <https://doi.org/10.1007/s11222-008-9104-9>.
- Thompson, B. K., J. D. Olden, and S. J. Converse. 2021. "Mechanistic Invasive Species Management Models and their Application in Conservation." *Conservation Science and Practice* 3(11): e533. <https://doi.org/10.1111/csp2.533>.
- Travis, J. M. J., K. Mustin, K. A. Bartoni, T. G. Benton, J. Clobert, M. M. Delgado, C. Dytham, et al. 2012. "Modelling Dispersal: An Eco-Evolutionary Framework Incorporating Emigration, Movement, Settlement Behaviour and the Multiple Costs Involved." *Methods in Ecology and Evolution* 3(4): 628–641. <https://doi.org/10.1111/j.2041-210X.2012.00193.x>.
- Urban, M. C., G. Bocedi, A. P. Hendry, J. B. Mihoub, G. Pe'er, A. Singer, J. R. Bridle, et al. 2016. "Improving the Forecast for Biodiversity under Climate Change." *Science* 353: 6304. <https://doi.org/10.1126/science.aad8466>.
- Valavi, R., J. Elith, J. J. Lahoz-Monfort, and G. Guillera-Arroita. 2019. "blockCV: An r Package for Generating Spatially or Environmentally Separated Folds for k-Fold Cross-Validation of Species Distribution Models." *Methods in Ecology and Evolution* 10(2): 225–232. <https://doi.org/10.1111/2041-210X.13107>.
- Vehtari, A., A. Gelman, and J. Gabry. 2017. "Practical Bayesian Model Evaluation Using Leave-One-out Cross-Validation and WAIC." *Statistics and Computing* 27(5): 1413–32. <https://doi.org/10.1007/s11222-016-9696-4>.
- Vehtari, A., A. Gelman, D. Simpson, B. Carpenter, and P.-C. Bürkner. 2021. "Rank-Normalization, Folding, and Localization: An Improved \hat{R} for Assessing Convergence of MCMC (with Discussion)." *Bayesian Analysis* 16(2): 667–718. <https://doi.org/10.1214/20-BA1221>.
- Visintin, C., N. J. Briscoe, S. N. C. Woolley, P. E. Lentini, R. Tingley, B. A. Wintle, and N. Golding. 2020. "Steps: Software for Spatially and Temporally Explicit Population Simulations."

- Methods in Ecology and Evolution* 11(4): 596–603. <https://doi.org/10.1111/2041-210X.13354>.
- Watts, K., R. C. Whytock, K. J. Park, E. Fuentes-Montemayor, N. A. Macgregor, S. Duffield, and P. J. K. McGowan. 2020. “Ecological Time Lags and the Journey towards Conservation Success.” *Nature Ecology & Evolution* 4(3): 304–311. <https://doi.org/10.1038/s41559-019-1087-8>.
- Wenger, S. J., and J. D. Olden. 2012. “Assessing Transferability of Ecological Models: An Underappreciated Aspect of Statistical Validation.” *Methods in Ecology and Evolution* 3(2): 260–67. <https://doi.org/10.1111/j.2041-210X.2011.00170.x>.
- Wikle, C. K. 2003. “Hierarchical Bayesian Models for Predicting the Spread of Ecological Processes.” *Ecology* 84(6): 1382–94.
- Zurell, D., C. König, A.-K. Malchow, S. Kapitza, G. Bocedi, J. Travis, and G. Fandos. 2022. “Spatially Explicit Models for Decision-Making in Animal Conservation and Restoration.” *Ecography* 2022: 4. <https://doi.org/10.1111/ecog.05787>.
- Zylstra, E. R., and E. F. Zipkin. 2021. “Accounting for Sources of Uncertainty when Forecasting Population Responses to

Climate Change.” *Journal of Animal Ecology* 90(3): 558–561. <https://doi.org/10.1111/1365-2656.13443>.

SUPPORTING INFORMATION

Additional supporting information can be found online in the Supporting Information section at the end of this article.

How to cite this article: Malchow, Anne-Kathleen, Guillermo Fandos, Urs G. Kormann, Martin U. Grüebler, Marc Kéry, Florian Hartig, and Damaris Zurell. 2024. “Fitting Individual-Based Models of Spatial Population Dynamics to Long-Term Monitoring Data.” *Ecological Applications* 34(4): e2966. <https://doi.org/10.1002/eap.2966>